Journal of Membrane Science 555 (2018) 483–496

Contents lists available at ScienceDirect

Journal of Membrane Science

journal homepage: www.elsevier.com/locate/memsci

Temperature and pressure dependence of gas permeation in amine-modified PIM-1

Bekir Satilmis[a,b], Marek Lanč[c], Alessio Fuoco[d], Carmen Rizzuto[d], Elena Tocci[d], Paola Bernardo[d], Gabriele Clarizia[d], Elisa Esposito[d], Marcello Monteleone[d], Marcela Dendisová[c], Karel Friess[c], Peter M. Budd[a,*], Johannes C. Jansen[d,*]

[a] School of Chemistry, University of Manchester, Manchester M13 9PL, UK
[b] Department of Chemistry, Ahi Evran University, Kirsehir 40100, Turkey
[c] Department of Physical Chemistry, University of Chemistry and Technology Prague, Technická 5, Prague 6 166 28, Czech Republic
[d] Institute on Membrane Technology (ITM-CNR), Via P. Bucci, 17/C, 87036 Rende, CS, Italy

ARTICLE INFO

Keywords:
Polymer of intrinsic microporosity
Gas separation
Gas sorption
Molecular modelling
Carbon dioxide

ABSTRACT

Polymers of intrinsic microporosity (PIMs) are among the most promising candidates for the development of novel polymeric gas separation membranes for processes such as carbon capture and storage, natural gas treatment and biogas upgrading. As one of the approaches to optimize their performance, PIMs are functionalized by CO_2-philic groups to improve the CO_2 separation by the enhancement of specific noncovalent interactions. In this work, we show the preparation of amine-PIM from the archetypal PIM-1, using borane dimethyl sulphide complexes in order to control the degree of conversion. The PIM-1 to amine-PIM-1 conversion was characterized by ATR-IR and NMR analysis. The influence of the amine moiety on the gas transport behaviour was investigated by two complementary techniques: gas permeation measurements by the time lag method and analysis of the sorption kinetics and the equilibrium sorption isotherms by the gravimetric method. Both techniques show that permeability decreases with increasing degree of conversion. The trends in the indirectly calculated solubility confirm those of direct analysis, although quantitative comparison of the two shows fundamental differences. A pressure and temperature study on a fully converted sample indicates that the solution-diffusion model should be expressed in concentration dependent transport parameters to be correct. The experimental work was supported by quantum mechanics studies and by molecular dynamics simulations to confirm the selective non-covalent interaction of CO_2 with the amino groups.

1. Introduction

Polymeric membrane technology is a promising technology for carbon capture and storage (CCS) because of its smaller footprint with respect to traditional technologies. To date, a membrane based solution for CCS is not economically viable due to the low gas fluxes through commercially available membranes [1]. Very large gas volumes and relatively low carbon dioxide concentrations make the capture the most expensive operation in the overall CCS process, accounting for about 70% of the overall cost [2]. Therefore, new materials with high permeability and good selectivity, are needed to reduce the membrane surface area and the related capital costs. The gas permeability of Polymers of Intrinsic Microporosity (PIMs) is orders of magnitude higher with respect to traditional materials for gas separation membranes, such as polyimides and polysulfones, but their moderate selectivity must be enhanced for allowing them to become the next-generation materials for CCS solutions.

The archetypal Polymer of Intrinsic Microporosity, commonly termed PIM-1, was first reported by Budd and McKeown [3,4]. It is easily processable, soluble in common organic solvents and forms robust membranes by solvent evaporation. Its permselectivity lies on the 2008 Robeson's upper bound. The nitrile groups in the PIM-1 structure provide a great opportunity for post modifications and for synthesis of new polymers [5–15]. Knowing that amine scrubbing is the traditional separation process most used in CCS, the functionalization of PIM-1 with N-containing groups is the natural step forward to increase the solubility of CO_2 with respect to the other gases. Du et al. [5] report the modification of PIM-1 via conversion of the nitrile group into a tetrazole unit by cycloaddition to form so-called TZPIMs. The TZPIMs exhibited exceptional gas separation performance with improved CO_2/N_2

* Corresponding author.
E-mail addresses: Peter.Budd@manchester.ac.uk (P.M. Budd), johannescarolus.jansen@cnr.it (J.C. Jansen).

https://doi.org/10.1016/j.memsci.2018.03.039
Received 24 January 2018; Received in revised form 13 March 2018; Accepted 17 March 2018
Available online 20 March 2018
0376-7388/

selectivity, especially in gas mixtures. While the polymer selectively sorbs CO_2 molecules, transportation of N_2 molecules is hindered. Despite the exceptional separation performance of TZPIMs, the membranes become too brittle above 70% conversion to enable successful gas separation measurements. Subsequently, it was found that methylation of tetrazole group reduced the hydrogen bonding ability between polymer and solvent, leading to enhanced mechanical properties (MTZ-PIMs) [6]. The solubility of the polymer was enhanced by the addition of the methyl group, and methyl tetrazole PIM is soluble in both protic and aprotic solvents, which gives better processability than the dimethylacetamide-soluble tetrazole analogue. However, methylation caused a decrease in permeability and MTZ-PIMs displayed lower CO_2 permeability and a lower CO_2/N_2 ideal selectivity, but similar mixed gas selectivity compared to TZPIMs. Mason et al. [8] reported thioamide functionalization in order to enhance interaction ability of PIM-1 with penetrant species, particularly with CO_2. With the aid of a thionating agent and in the presence of sodium sulphide, the nitrile group of PIM-1 was converted to the corresponding thioamide. The resulting polymer was soluble in THF. Thus, solution processability was preserved after modification. Similar to other modifications, thioamide functionalization improves the gas selectivity of PIM-1 but reduces the permeability. Recently, Patel et al. [10] introduced the amidoxime functionality, which gives enhanced CO_2 uptake, possibly by an increased micropore surface area, as a result of the transformation of some of the mesopores into micropores. Swaidan *et al.* [13] reported the gas separation performance of amidoxime-PIM in which a loss of permeability resulted in a threefold increase in CO_2/CH_4 mixed gas selectivity.

We have previously reported the use of borane complexes to fully reduce the nitrile groups in PIM-1 to primary amines [11]. In the present paper, we show the controlled conversion of PIM-1 into amine-PIM-1, and the effect on the CO_2 affinity and gas transport properties. The correlation between the transport properties and the conversion highlights the role of the amine groups on the transport properties. Temperature and pressure dependences of the gas transport properties of a membrane with high amino content provide further insight into its somewhat unusual behaviour previously observed [11]. Molecular modelling was used to support the experimental findings.

2. Materials and methods

2.1. Materials

Methanol, ethanol (> 99.5%), Dimethylacetamide (DMAc), toluene, chloroform (≥ 99.5%, stabilised with amylene) and borane dimethyl sulphide complex (5.0 M solution in diethyl ether) were purchased from Sigma-Aldrich and used without further purification. Tetrafluoroterephthalonitrile (TFTPN, 98%, Aldrich) was purified by sublimation around 150 °C without vacuum. 5,5′,6,6′-Tetrahydroxy-3,3,3′,3′-tetramethyl-1,1′-spirobisindane (TTSBI, 98%, Alfa Aesar) was purified before, dissolving it in methanol and re-precipitating from dichloromethane. Anhydrous potassium carbonate (K_2CO_3, 99.0%, Fisher) was dried overnight at 110 °C in an oven.

2.2. Synthesis

2.2.1. Amine modification of PIM-1 powder

PIM-1 (M_w = 157,000 g mol^{-1}, M_w = 49,000 g mol^{-1}) was synthetized as reported previously [12]. PIM-1 (3 g) was placed into a dry three-neck, round-bottom flask under an inert nitrogen atmosphere and 5 M borane dimethyl sulphide complex (40 mL) was added. The reaction was set to reflux (45 °C) and samples were taken periodically. After cooling, the excess borane was deactivated by adding ethanol (40 mL) and the mixture was stirred overnight. The samples were filtered under vacuum and soaked in 1 M methanolic HCl overnight to remove any trace of boron, then filtered again and stirred in 5% (w/w) aqueous sodium hydroxide for a further night to neutralise the polymers. After the filtration of this product it was washed with deionized water continuously until it was neutral. It was oven dried at 110 °C overnight to yield a pale yellow powder. Reaction times and temperatures are given SI Table 1.

2.2.2. Amine modification of PIM-1 membranes

Fresh PIM−1 membranes were used for synthesis, and their thicknesses are reported in Table 2 and SI Table 2. PIM−1 [12] membranes (3 membranes of 0.3 g each) were placed in a dry flange reactor and the membranes were separated from each other by capillary rods. The lid was greased and the reactor assembled before fitting with condenser, nitrogen inlet and septum. The reactor was placed in an oil bath, which was heated before adding the complex. Borane-dimethylsulphide complex (90 mL, 5 M in diethyl ether) was added by a glass syringe. The reaction was then set to reflux (45 °C) for a certain period. At the end of the reaction, the excess borane was decanted off and ethanol added carefully, dropwise, to the membranes. The membranes were left in ethanol (400 mL) overnight. The membranes were then soaked in 1 M methanolic HCl (400 mL) overnight, followed by 5% (w/w) aqueous sodium hydroxide (800 mL) for a further night to neutralise the membrane. Following this, membranes were soaked in water and washed repeatedly (3 times in 500 mL). Membranes were finally dried overnight at 110 °C in an oven to give pale yellow membranes. Further samples (designated F in the code in SI Table 2) were prepared following the same procedure with 80 mL borane-dimethylsulphide complex and 600 mL NaOH. Reaction times and temperatures for all membrane samples are given in Table 1.

2.3. Characterization

2.3.1. Polymer characterization

Infrared (IR) spectra of samples were recorded on a Thermo Scientific™ Nicolet iS5 FT-IR Spectrometer with an Attenuated Total Reflectance (ATR) accessory, taking 16 scans of each sample at a resolution of 4 cm^{-1}. Peak areas were determined by means of the Omnic software.

Raman spectra were collected using a Renishaw *InVia Reflex* dispersive Raman spectrometer (United Kingdom), equipped with a diode laser, emitting radiation at 785 nm, x-y-z positioning stage, grating with 1200 lines mm^{-1} and a thermoelectrically cooled CCD detector. Each spectrum was recorded as 10 accumulations with 60 s integration time per acquisition and the final spectrum was averaged over 5 acquisitions, using a laser power of 1 mW and a 100 × objective. Spectra were collected in the spectral range from 100 to 3100 cm^{-1} and corrected with WiRe software. Depth measurements were carried in 8 layers with 10 μm steps, taking 4 points at distances of 70 μm from each other.

High powered decoupling (Hpdec) solid state NMR spectra of

Table 1
Ratio of C≡N to C−H from ATR-IR spectra, I_{CN}/I_{CH}, and conversion in PIM-1 and amine-modified PIM-1 membranes as function of the reaction conditions. Where A stands for "amine-PIM-1", M for "membrane" and the number is the average conversion of the cyano group into the amine (in %).

Sample	*Reaction temperature* (°C)	*Reaction time* (min)	I_{CN}/I_{CH}	Conversion (%)
PIM−1			0.07	0
AM_12	20	20	0.06	12
AM_64	45	20	0.022	64
AM_84	45	70	0.009	84
AM_85	45	40	0.009	85
AM_91	45	70	0.005	91
AM_92	45	1260	0.005	92
AM_93a	45	630	0.004	93
AM_93b	45	40	0.004	93
AM_97	45	630	0.002	97

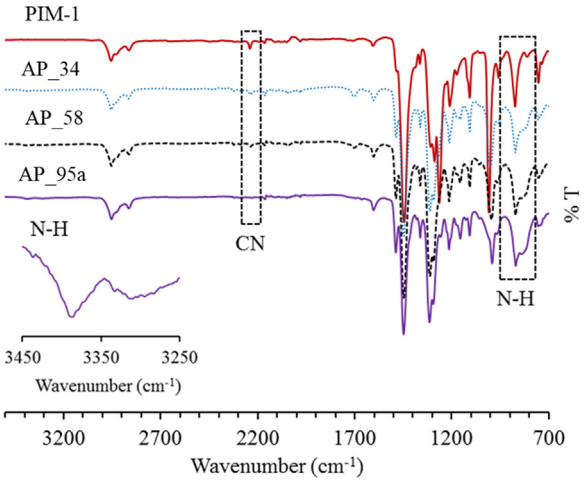

Fig. 1. ATR-IR spectra of PIM-1 (top) and amine-modified PIM-1 (Reaction times: AP_34, 40 min; AP_58, 60 min; AP_95a, 120 min). Inset is an expansion of the region 3250–3450 cm^{-1} for sample AP_95a.

powder and membrane samples in a 4 mm zirconium rotor were recorded on a Bruker Avance III 400 MHz instrument under magic angle spinning (MAS). Spectra were compiled from 6000 scans, using a repetition time of 10 s and a spectral width of 600 ppm at a spinning rate of ~10,000 Hz, using an adamantane reference.

Elemental CHNS analysis was done with a Thermo Scientific Flash 2000 organic elemental analyser. For boron analysis, samples were weighed, acid digested in a mixture of Nitric, Sulphuric and Perchloric acid at 320 °C and made up into an aqueous solution. The boron concentration in solution was measured using a Thermo Scientific iCAP 6300 Duo ICP Spectrometer.

Thermogravimetric Analysis (TGA) of polymer samples was performed on a Mettler Toledo Star System under nitrogen at a heating rate of 10 °C min^{-1}, up to 1000 °C.

2.3.2. Gas sorption

CO_2 and N_2 adsorption isotherms of ca. 0.1 g of powdered samples were measured up to 8 bar at 0 °C on a Micromeritics ASAP 2050 surface area and porosity analyser. The powder sample was degassed under high vacuum at 120 °C for 16 h, weighed accurately, and further degassed for 2 h under high vacuum to ensure complete removal of all volatiles before adsorption analysis. Samples were then degassed again for 2 h and a free space measurement was carried out using helium.

Gravimetric sorption experiments of CO_2, CH_4 and N_2 at 25.0 ± 0.1 °C were performed as described previously [16], using a robust home-made apparatus equipped with a calibrated McBain quartz spiral balance. The sample in the thick-walled glass measuring tube was evacuated ($< 10^{-3}$ mbar) before each measurement by a rotary oil pump (Leybold Trivac D4B) with an oil-mist filter until constant weight. The quartz spiral elongation was recorded by a charge-coupled device (CCD, Sony), allowing determination of the gravimetric sorption with a maximum experimental error of ca. 30 micrograms [17]. For the samples used in this work, this corresponds to less than 0.5% error for CO_2 sorption and less than 3% error for CH_4 sorption. The detailed description of the experimental procedure and the apparatus calibration were described previously [16]. The diffusion coefficients were evaluated via non-linear regression of the sorption kinetics curves, using a fitting function based on Fick's second law of diffusion. Under the appropriate initial and boundary conditions (zero initial gas concentration in a membrane; step pressure increase from 0 to relative pressure 1 in the sorption cell at $t = 0$; constant gas concentration around the membrane at $t > 0$), the relationship between the relative sorption amount Q_t/Q_∞ and time t for a membrane with thickness l can be expressed by [18]:

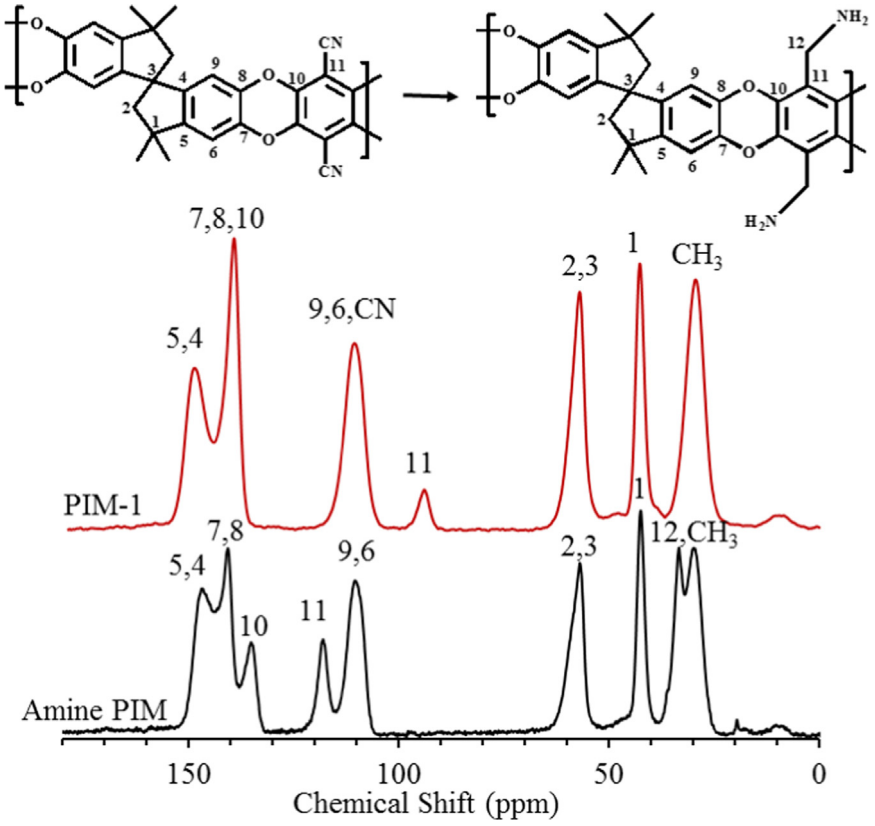

Fig. 2. Solid state ^{13}C-NMR spectra of PIM-1 (top) and amine-PIM-1 sample AP_95c (bottom).

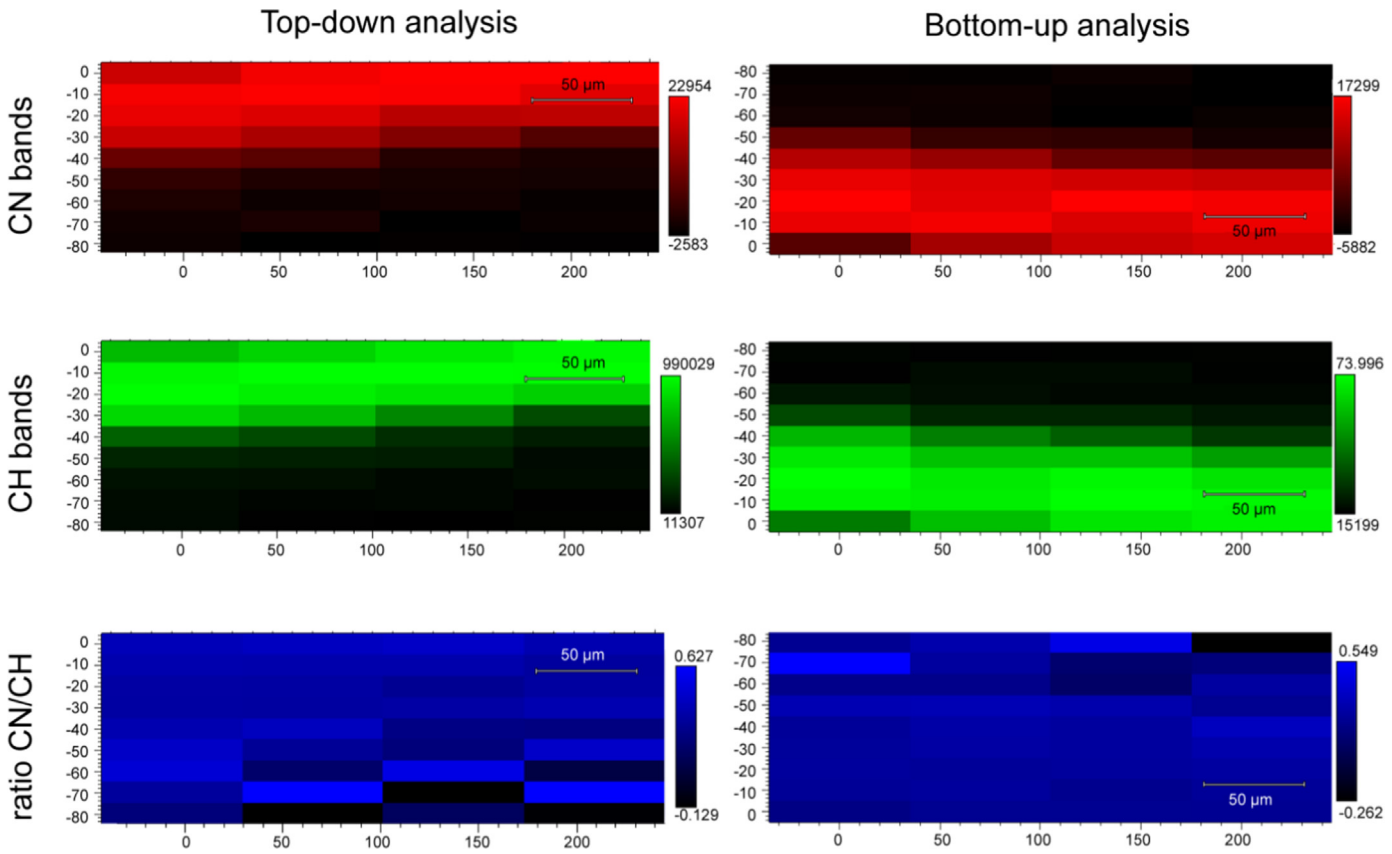

Fig. 3. Depth spectral maps of the ca. 80 µm thick membrane AM_85 with 85% conversion, showing the CN bands (top) and the aliphatic C-H stretching modes (middle) upon analysis from the top side down (left) and from the bottom side up (right). The bottom image shows the ratio of CN/CH modes obtained via a combination of the single signals. The top layer of the membrane corresponds to a value 0 of the y-axis and the brighter the colour in the map, the higher the intensity of the signal. Black areas with zero intensity are an artefact, representing the reflections from the glass support of the membrane with weak signal of the sample.

$$\frac{Q_t}{Q_\infty} = 1 - \frac{8}{\pi^2}\sum_{n=0}^{\infty}\frac{1}{(2n+1)^2}\cdot e^{-\frac{D\cdot(2n+1)^2\cdot\pi^2\cdot t}{l^2}} \quad (1)$$

Eq. (1) is limited to one-dimensional diffusion, assuming that the diffusion process is symmetrical from both sides of the membrane and negligible through the edges, because the cross-sectional area is much smaller than the membrane surface area. Actually, the assumed condition of the step-pressure-increase in Eq. (1) cannot be fulfilled in real measurement due to the experimental setup and procedure. Therefore, the double exponential relative pressure increase step approach (Eq. (2)), derived by Vopička et al. [17], was used:

$$p_{rel} = 1 - \exp(-\xi t) - \xi t\cdot\exp(-\xi t) \quad (2)$$

in which ξ is a fitting parameter. The relationship between the relative sorption amount Q_t/Q_∞ and time t is given by:

$$\frac{Q_t}{Q_\infty} = 1 - \exp(-\xi t) - \xi t\cdot\exp(-\xi t)$$
$$- \frac{8}{\pi^2}\cdot\sum_{i=0}^{\infty}\left[\frac{1}{(2i+1)^2}(A\cdot\exp(-dt\cdot(2i+1)^2) + (Ct - A)\cdot\exp(-\xi t))\right]$$
$$A = \frac{\xi^2}{\xi^2 - 2\xi d\cdot(2i+1)^2 + d^2\cdot(2i+1)^4}$$
$$C = \frac{\xi^2}{d\cdot(2i+1)^2 - \xi}$$
$$d = \frac{\pi^2\cdot D}{l^2} \quad (3)$$

The overall error in the diffusion coefficient determination by gravimetric sorption, related to the experimental conditions and to the standard deviation in the thickness, is less than 10%.

2.3.3. Gas permeation

Single gas permeation measurements at 25 °C and 1 bar feed pressure were carried out in the time lag mode in a barometric apparatus (GKSS, Germany) described previously [19], while the measurements at variable temperature and pressure were performed in an improved setup (EESR, Germany) [20] with turbomolecular pump instead of a rotary pump with oil mist filter. Circular membranes with 2.14 cm^2 effective area were carefully degassed under vacuum before each run. The gases were tested in the following order: He, H_2, N_2, O_2, CH_4, and CO_2 on "as prepared" and "MeOH treated" samples. The treatment in methanol was carried out as follows. Each membrane sample was soaked in methanol overnight, removed from the MeOH and dried for 24 h at ambient conditions between two porous sintered glass disks to avoid curling. The permeation tests were carried out on the consecutive day. The sample was degassed for at least one hour inside the permeation cell before the gas testing. A digital micrometer (Mitutoyo, model IP65) was used to determine the thickness of the membranes. The permeability coefficient, P (barrer), and diffusion coefficient, D (m^2 s^{-1}), were determined as described previously [19], and the solubility coefficient, S (cm^3(STP) cm^{-3} bar^{-1}), was indirectly evaluated as the ratio P/D. The ideal permselectivity for different gas pairs was calculated as the ratio of the individual single gas permeabilities or as the product of the diffusion selectivity and solubility selectivity:

$$\alpha_{A/B} = \frac{P_A}{P_B} = \frac{S_A}{S_B}\cdot\frac{D_A}{D_B} \quad (4)$$

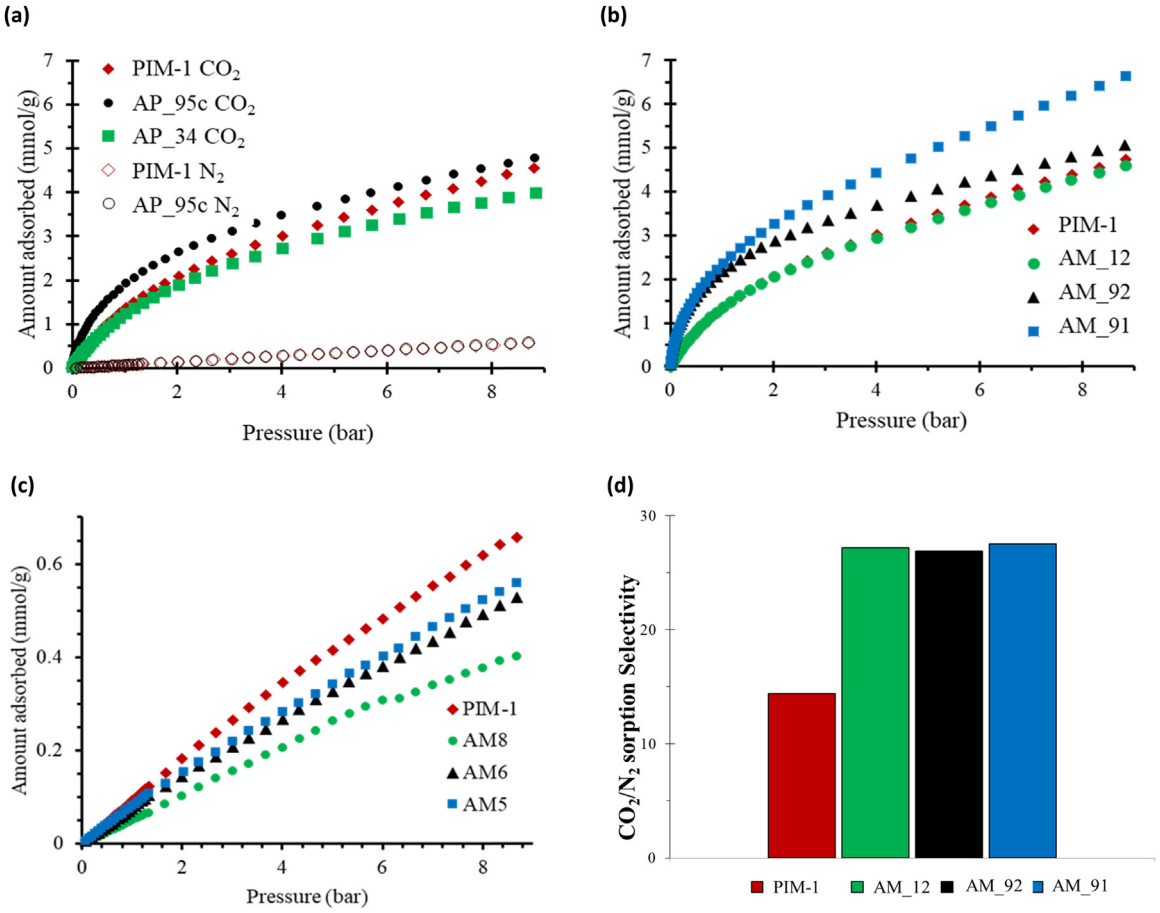

Fig. 4. Representative adsorption isotherms of (a) CO_2 (filled symbols) and N_2 (empty ○ symbols) at 0 °C in PIM-1 powder (◆), amine-modified PIM-1 powder AP_95c (•) and partially-modified (34%) powder AP_34 (■). Representative CO_2 (b) and N_2 (c) adsorption isotherms at 0 °C of PIM-1 membrane (◆) and amine-modified PIM-1 membranes AM_12 (●), AM_92 (▲) and AM_91 (■). (d) Ideal CO_2/N_2 sorption selectivity at 1 bar.

2.4. Molecular modelling

2.4.1. Molecular dynamics simulations

The Material Studio package (version 7.0) of Accelrys [21] and the COMPASS (Condensed-phase Optimized Molecular Potentials for Atomistic Simulation Studies) force field [22] were used for all simulations of the amorphous membrane models. COMPASS was used with success in several MD simulations of PIM-related materials [23–26]. The amine-PIM-1 template chain for the initial packing with the Amorphous Cell module consisted of 30 monomers (1860 atoms) and every packing model contained three polymer chains. Thus, a total of 5580 atoms were grown in a 3D model under periodic boundary conditions. Temperature was set at 298 K whilst the initial density was 0.1 g cm^{-3}. Moreover, 300 randomly distributed Ar atoms were inserted as obstacles in the 3D models during the Monte Carlo chain growth stage. Those molecules were later removed during optimization of the structures. This procedure avoided the possibility to create artificially ring catenations and spearings. More details on the method for packing and equilibration can be found in ref. [27]. The Amorphous-Cell module [21] was employed to build amorphous polymer model using the method of Theodorou/Suter [28,29]. The structures were relaxed, applying a scheme that includes the force field parameter-scaling [27]. After the removal of the obstacle molecules, energy minimization and molecular dynamics (MD) runs were carried out for each parameter set, using the NVT ensemble based on constant number of particles, volume and temperature. Then, to increase the density of packing models a set of MD runs were performed. Final equilibration was performed by a long *NpT*-MD run at constant temperature, pressure and number of particles [27]. The initial velocities were randomly evaluated, setting the time step to 1 femtosecond (fs) and keeping the temperature and pressure constant, using the Berendsen method [30]. The Group Based method was used for controlling long-range Coulomb and van der Waals interactions. The procedure was repeated for the generation of realistic amorphous cells, eliminating the non-realistic boxes. The side lengths of the packing cells were of 39.068 Å and a final density was of 1.19 $\pm$ 0.01 g cm^{-3}. In the absence of experimental evidence, swelling or plasticization are not taken into account in the molecular modelling either.

2.4.2. Quantum mechanics calculations

The interaction energies between the amine-PIM-1 monomer and CO_2, N_2 and CH_4 molecules were investigated by quantum mechanics (QM). The QM calculations were performed by NWChem 6.5 [31] in the framework of Density Functional Theory (DFT) and using B3LYP functional [32,33]. Double-ζ basis sets with polarization and diffusion functions were used for the geometry optimization without any constraints. The convergence criteria based on Cartesian displacement and gradient thresholds were set as default [34]. Basis set super position error (BSSE) correction [35] was applied in the computing of interaction energies between the polymer and the gas.

3. Results and discussion

3.1. Characterization of amine-PIM-1 powders

In previous work [11], both borane tetrahydrofuran and borane

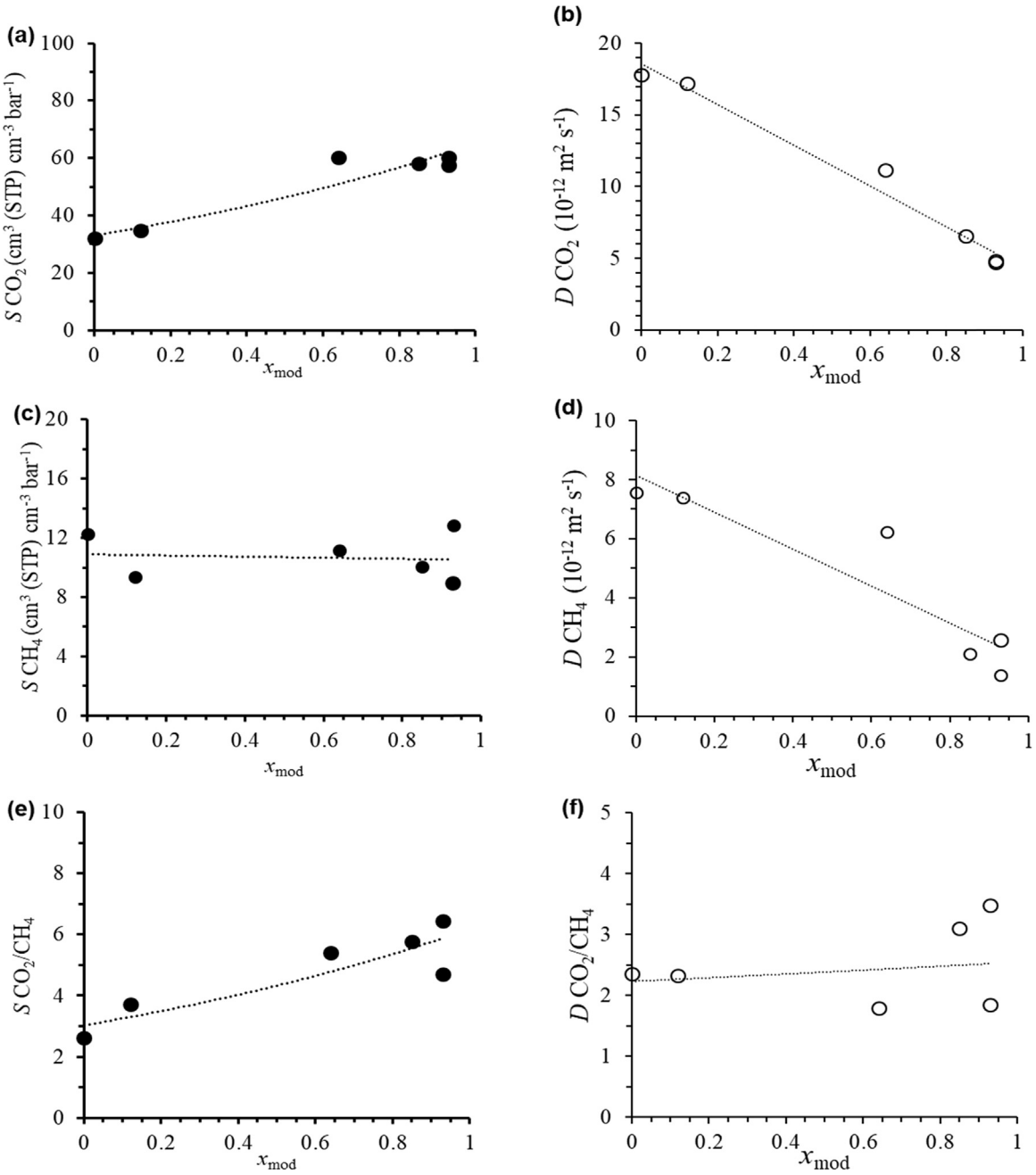

Fig. 5. CO_2 and CH_4 sorption (left) and diffusion (right) coefficients with their related selectivities, determined by gravimetric sorption for amine-modified PIM-1 membranes as a function of the conversion. Measurements performed after MeOH treatment. Trend lines are plotted as a guide to the eye.

dimethyl sulphide complexes were used to reduce nitrile to primary amine. However, the tetrahydrofuran complex has been found to give variable results, so the dimethyl sulphide complex was used exclusively in this work. A possible mechanism for the reaction was proposed by Brown *et al.* [36]. Although the parent polymer PIM-1 is soluble in solvents such as $CHCl_3$ and tetrahydrofuran, the modified polymers, which slightly change colour (SI Fig. 1) were insoluble in all common laboratory solvents tested, as reported previously [11]. Thus, the reaction products could not be characterized in solution.

Attenuated Total Reflectance Infrared (ATR-IR) spectra in Fig. 1 show that the nitrile stretch (ca. 2240 cm^{-1}) is lost after 120 min reaction time. New peaks appear at 3360 cm^{-1} and 800 cm^{-1}, which may be assigned as N-H stretch and N-H wag, respectively. The degree of conversion was determined from the area of the C≡N peak at 2257–2220 cm^{-1}, I_{CN}, and the area of the C-H region at 2818–3018 cm^{-1}, I_{CH}. For a partially-modified polymer with mole fraction of nitrile units x_{CN}, the area of the nitrile peak, $(I_{CN})_{mod}$, will relate to that of the parent polymer, $(I_{CN})_{PIM\text{-}1}$ by the equation:

$$(I_{CN})_{mod} = x_{CN} \times f \times (I_{CN})_{PIM-1} \quad (5)$$

where f is a scaling factor, calculated from the ratio of an independent peak in the two different samples, to normalize for systematic differences between measurements. In PIM-1, for each nitrile there are two aromatic C-H and eight aliphatic C-H groups (i.e., 10C-H in total). On modification one CH_2 group (i.e., 2 C-H) is formed for each nitrile lost. Assuming that aromatic and aliphatic C-H contribute equally to the area of the C-H region, for fully modified polymer I_{CH} is 1.2 times that of unmodified polymer. Hence, for a partially-modified polymer, the area of the C-H region, $(I_{CH})_{mod}$, will relate to that for the parent polymer, $(I_{CH})_{PIM\text{-}1}$, by:

Table 2
Gas permeability, diffusion, and solubility coefficients, and related selectivities of PIM-1 and amine-PIM − 1 membranes after MeOH treatment.

	Thickness (μm)	Permeability (barrer)						Permeability Selectivity (-)			
Sample		CO_2	He	H_2	CH_4	O_2	N_2	H_2/CO_2	H_2/N_2	CO_2/N_2	CO_2/CH_4
PIM − 1	69	12100	2000	4980	914	2140	607	0.41	8.20	19.9	13.2
AM_12	75	5670	1270	2920	463	1030	284	0.51	10.3	20.0	12.2
AM_64	63	8190	1610	3880	586	1380	394	0.47	9.84	20.8	14.0
AM_84	53	1590	846	2150	161	567	132	1.35	16.3	12.0	9.88
AM_85	90	3040	1080	2850	531	1010	318	0.94	8.96	9.55	5.72
AM_91	96	1450	862	2280	359	752	210	1.57	10.9	6.93	4.05
AM_92	84	785	805	1810	178	550	132	2.31	13.7	5.95	4.41
AM_93a	76	1740	1060	2620	256	756	167	1.51	15.7	10.4	6.80
AM_93b	81	1170	792	1990	257	606	167	1.71	11.9	6.99	4.54
AM_97	100	1030	838	2180	240	664	176	2.13	12.4	5.83	4.28
		Diffusion coefficient (10^{-12} m^2 s^{-1})						Diffusion Selectivity (-)			
Sample		CO_2	He	H_2	CH_4	O_2	N_2	H_2/CO_2	H_2/N_2	CO_2/N_2	CO_2/CH_4
PIM − 1		153	2140	2270	41.2	406	133	14.8	17.0	1.15	3.71
AM_12		68.0	2230	2530	19.9	189	54.1	37.2	46.8	1.26	3.42
AM_64		72.9	5060	2770	23.2	190	64.8	38.0	42.7	1.12	3.14
AM_84		25.6	3900	2590	7.7	112	28.7	101	90.3	0.89	3.32
AM_85		61.3	4960	3800	22.7	212	70.0	62.0	54.3	0.87	2.70
AM_91		29.3	3590	2920	11.1	162	46.9	99.5	62.2	0.62	2.64
AM_92		24.8	3190	2430	6.8	107	28.0	98.0	86.7	0.88	3.65
AM_93a		30.5	2100	2340	11.0	131	33.3	77.0	70.3	0.91	2.77
AM_93b		20.0	2710	2380	12.5	126	36.2	119	65.9	0.55	1.60
AM_97		24.2	3540	2860	9.0	150	39.0	118	73.4	0.62	2.68
		Solubility (cm^3 (STP) cm^{-3} bar^{-1})						Solubility Selectivity (-)			
Sample		CO_2	He	H_2	CH_4	O_2	N_2	H_2/CO_2	H_2/N_2	CO_2/N_2	CO_2/CH_4
PIM − 1		59.4	0.70	1.65	16.6	3.96	3.41	0.028	0.48	17.4	3.56
AM_12		62.6	0.43	0.86	17.4	4.08	3.94	0.014	0.22	15.9	3.59
AM_64		85.2	0.24	1.05	19.0	5.47	4.56	0.012	0.23	18.7	4.49
AM_84		46.6	0.16	0.62	15.7	3.77	3.44	0.013	0.18	13.5	2.97
AM_85		37.1	0.16	0.56	17.6	3.57	3.41	0.015	0.16	10.9	2.11
AM_91		37.2	0.18	0.59	24.3	3.48	3.35	0.016	0.17	11.1	1.53
AM_92		23.7	0.19	0.56	19.5	3.86	3.55	0.024	0.16	6.70	1.22
AM_93a		42.9	0.38	0.84	17.5	4.31	3.76	0.019	0.22	11.4	2.45
AM_93b		43.7	0.22	0.63	15.4	3.60	3.47	0.014	0.18	12.6	2.84
AM_97		31.7	0.18	0.57	20.1	3.33	3.40	0.018	0.17	9.34	1.58

$$(I_{CH})_{mod} = f\,[(I_{CH})_{PIM-1} + 0.2(I_{CH})_{PIM-1}(1 - x_{CN})] = f\,(I_{CH})_{PIM-1}[1.2 - 0.2x_{CN}] \quad (6)$$

Hence, the mole fraction of nitrile units can be calculated from the IR data using Eq. (7).

$$x_{CN} = \frac{1.2\left(\frac{I_{CN}}{I_{CH}}\right)_{mod}}{\left(\frac{I_{CN}}{I_{CH}}\right)_{PIM-1} + 0.2\left(\frac{I_{CN}}{I_{CH}}\right)_{mod}} \quad (7)$$

The mole fraction of amino groups, x_{mod}, and the conversion are defined as:

$$x_{mod} = (1 - x_{CN}) \quad (8)$$

$$Conversion = (1 - x_{CN}) \times 100\% \quad (9)$$

The conversion increases with increasing temperature and increasing reaction time, and 2 h at 45 °C are sufficient to reach at least 95% conversion, while 6 h are needed to reach 88% conversion at room temperature (SI Table 1). These data are qualitatively confirmed by solid state ^{13}C-NMR spectroscopy (Fig. 2). Upon reaction, the new amine carbon (C12) signal appears at 33 ppm and the aromatic carbon which is attached to nitrile (C11) shifts from 95 ppm to 118 ppm, while aromatic carbon C10 shifts from 140 ppm to 136 ppm. The nitrile carbon signal overlaps with the aromatic carbon signals, so the loss of nitrile cannot be seen directly and must be confirmed by IR or Raman spectroscopy.

At intermediate reaction times, C11 is split into four different signals, which can be attributed to the aromatic carbon adjacent to (i) a nitrile in a unit with two nitriles, (ii) an amine in a unit with two amines, and (iii) a nitrile and (iv) an amine in a unit with both functional groups (Fig. 2). In addition, C12 appears in the aliphatic region and C10 shifts from its original region. Only at a high degree of conversion does C11 give a single peak at 118 ppm. For identification of the NMR peaks, a sample of AP_95b was also soaked in methanolic HCl (1 M) before ^{13}C-NMR analysis (SI Fig. 3). Protonation of the amino group causes a clear shift in peak C10 to 136 ppm, while C11 moves from 95 to 110 ppm, overlapping with the C9, C6 and CN peaks. After protonation, the signal of C12 disappears from the spectrum, as a confirmation of the conversion of the nitrile to the amino group.

3.2. Characterization of amine-PIM-1 membranes

Shrinkage occurred during the amine-PIM-1 membrane synthesis, due to the strong hydrogen bond interactions. It is usually around 5–10% in the diameter and thickness (SI Fig. 4). In a similar way as the powder samples, amine-modified membranes were characterized by ATR-IR and solid-state ^{13}C-NMR spectroscopy. Interestingly the IR spectra (SI Fig. 5) and the solid-state ^{13}C-NMR spectra (SI Fig. 6) show that the reaction proceeded more rapidly with the membranes than with the powder samples. The quantitative values of the conversion, calculated from IR data, are given in Table 1. Although the reaction conditions may play a role [36], most likely the faster reaction in the films is due to the packing of the polymer sample. It is likely that the fine powder has been more efficiently dried and has aged more rapidly than the thicker dense films. It is well known that the gas transport properties of PIMs depend dramatically on the sample treatment [37]. Permeation and sorption kinetics are also dramatically affected by aging of the sample [38], causing a decrease of the free volume. It is expected that sample history has a similar effect on the accessibility of the reactive sites in the polymer, and thus on the reaction rate. Indeed,

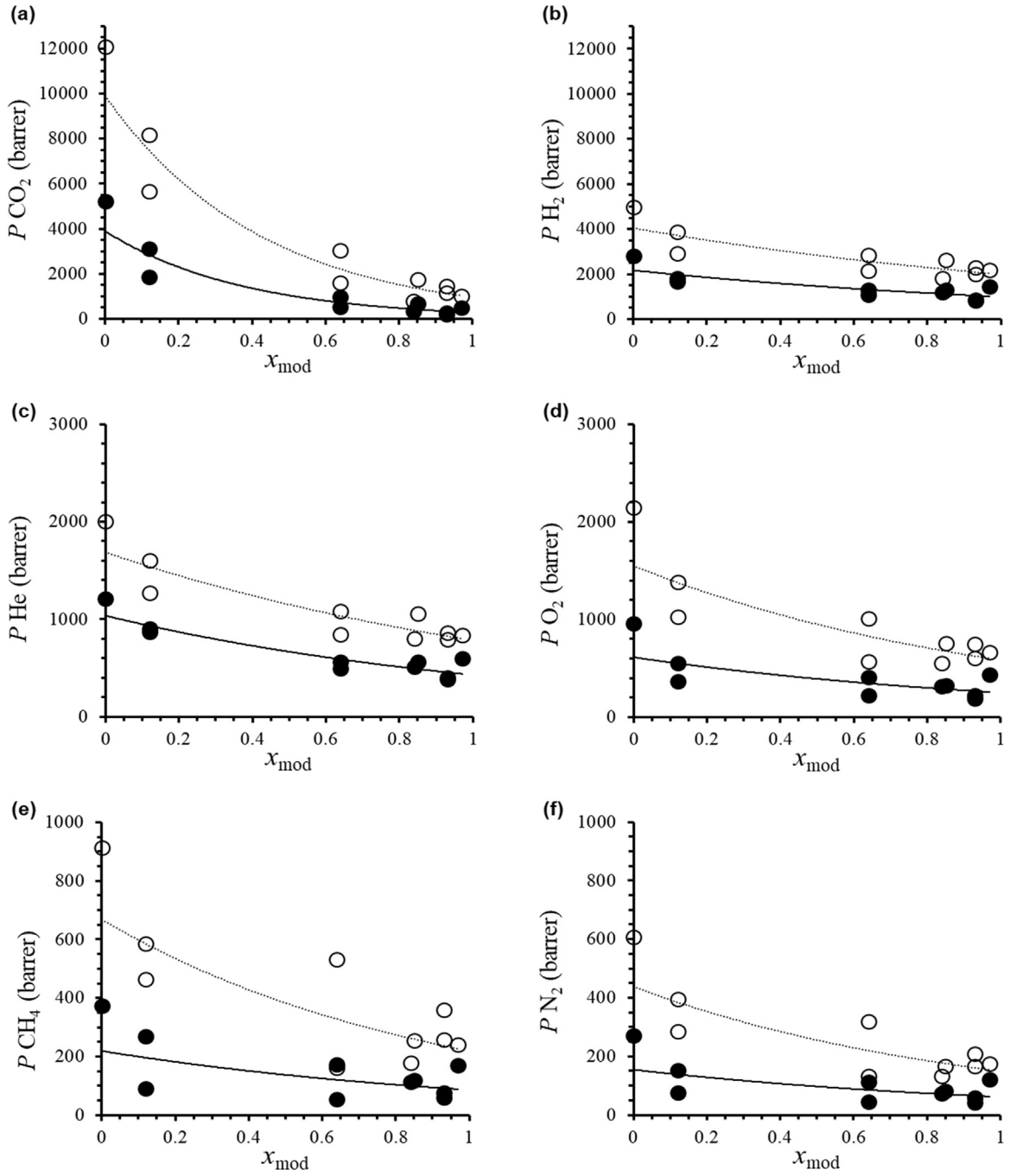

Fig. 6. Permeability coefficient, determined by the pressure-increase method, for amine-modified PIM-1 membranes as a function of the conversion. (a) CO_2, (b) H_2, (c) He, (d) O_2, (e) CH_4 and (f) N_2. (•) As prepared and (o) after MeOH treatment. Lines are indicated as a guide to the eye.

the conversion of the individual samples shows considerable scatter, but as a general trend it increases with increasing reaction time and temperature. The scatter is probably due to subtle differences in the samples, as a result of slight variations in their thermomechanical history before the reaction.

Since ATR-IR only probes the outer few micrometres of the samples, Raman spectroscopy with depth profiling was performed to confirm that the composition is homogenous through the entire thickness of the ca. 80 μm thick membrane. Depth measurements were carried out on a representative sample with 85% conversion (AM_85) over the whole thickness. The depth spectral maps of the C≡N vibration mode at 2240 cm^{-1} and the CN and CH signals from 2182 cm^{-1} to 2309 cm^{-1} and from 2824 cm^{-1} to 3015 cm^{-1}, respectively, were recorded from both sides of the membrane (Fig. 3). The map images clearly demonstrate that besides minor differences, the CH and CN signals are distributed evenly over the entire thickness of the membrane, and the CN/CH signal ratios are also almost constant along the cross section (Fig. 3, bottom). This confirms the uniform conversion of the nitrile groups through the whole membrane.

3.3. Gas transport properties

3.3.1. Gas sorption

Gas adsorption measurements of both methanol treated powders and membranes were conducted at 0 °C using a volumetric method. Powder samples (Fig. 4a) exhibit a higher uptake of CO_2 in the amine-

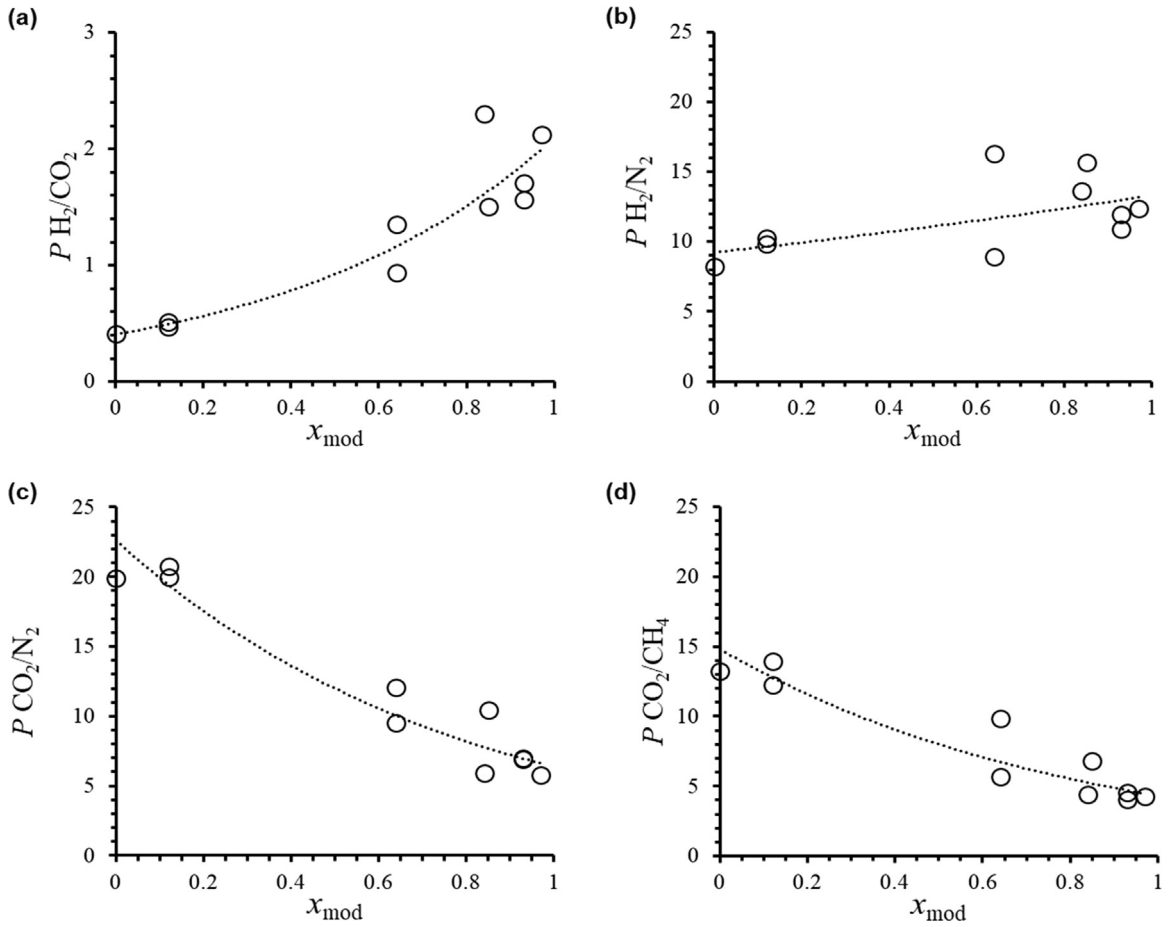

Fig. 7. Permselectivities in correlation with degree of modification for amine-modified PIM-1 membranes after MeOH treatment. (a) H_2/CO_2, (b) H_2/N_2, (c) CO_2/N_2 and (d) CO_2/CH_4. Lines are indicated as a guide to the eye.

modified (95%) PIM-1 than in the parent PIM-1 polymer, as previously reported [11], and the sorption isotherms show typical dual-mode behaviour, defined by the equation:

$$C_i = k_{Di}p_i + \frac{C'_{Hi}b_ip_i}{1 + b_ip_i} \quad (10)$$

where C_i is the gas concentration in the membrane at pressure p, k_{Di} is the Henry sorption constant, C'_{Hi} is the Langmuir sorption capacity and b_i is the affinity constant.

For the powders with high amino content, the ideal CO_2/N_2 sorption selectivity at 1 bar increased from 20 for PIM-1 to 27. Partially-modified (34%) PIM-1 shows slightly lower CO_2 uptake than the parent polymer, probably because the free volume is decreased by the inter- and intra-chain interaction of the polar amino groups, whereas the concentration of amino groups in the polymer is still too low to increase significantly the affinity for CO_2. Fig. 4b shows that amine-modified PIM-1 membranes have higher CO_2 uptake than the parent polymer, also here with the exception of the sample with low conversion (AM_12, 12% modified). As discussed previously [11], the strong interaction with CO_2 may reflect strong adsorption in ultramicropores (< 0.7 nm) and/or specific interactions with amine sites. AM_12 has slightly lower uptake than the parent polymer, as observed above for a powder sample with low conversion (AP_34).

Even though AM_92 and AM_91 have similar conversions, 92% and 91% respectively, they showed some difference at high pressure. AM6, for which the reaction time was much longer than for AM_91, shows a similar affinity for CO_2 at low pressures, but a smaller Henry contribution in the dual mode sorption behaviour. Apparently, the long reaction time reduces the ability of the polymer to swell in the presence of CO_2, possibly due to the formation of cross-links or of strong inter- and intra-chain interactions. N_2 adsorption isotherms of the membranes in Fig. 4c reveal reduced N_2 uptake for all amine-modified polymers compared to the parent polymer. Thus, the ideal CO_2/N_2 sorption selectivity increased for all the modified samples (Fig. 4d). Qualitatively, these trends are confirmed for the CO_2/CH_4 gas pair by gravimetric sorption measurements (Fig. 5). The experiments were carried out on a McBain quartz spiral balance, which allows also the determination of the sorption kinetics via time-resolved analysis of the sample weight. Interestingly, beside the selective increase in the CO_2 solubility upon conversion into the amine, there is a strong decrease in the diffusion coefficient of both CO_2 and CH_4.

3.3.2. Gas permeation

A complete overview of the transport parameters of the MeOH treated samples is given in Table 2, and the corresponding data for the 'as prepared' samples are given in the Supporting information, SI Table 2.

Fig. 6 shows the permeability coefficients determined by the pressure-increase method, for "as prepared" and "MeOH treated" membranes. After the modification, membranes became less permeable due to the introduced amine functional groups, which have noncovalent bonding ability similar to other PIM modifications [7,8]. The decrease in CO_2 permeability is more pronounced with respect to the other gases, probably due to the introduction of noncovalent interaction between the amine-groups and the polarized C = O bonds in the CO_2 molecules. Depending on the gas species, treatment of the polymers with MeOH gives a 2–3 fold increase of permeability due to the removal of the residual solvents and opening up of excess free volume [39–42].

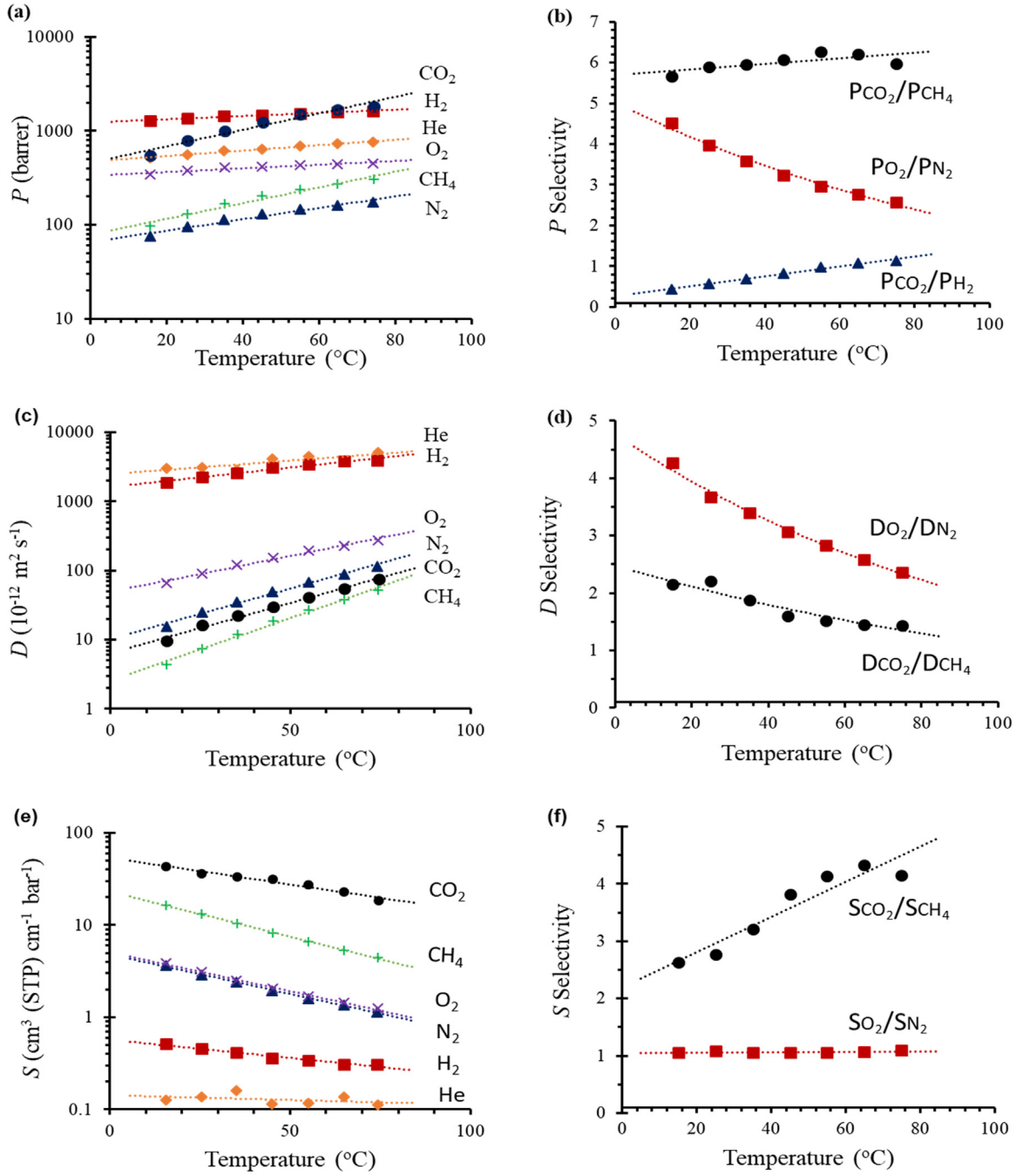

Fig. 8. Temperature dependence of (a) permeability, (c) diffusion, (e) solubility and (b) permselectivity, (d) diffusion selectivity and (f) solubility selectivity in membrane AM_93a. Related Arrhenius plots are reported in SI Figure 11.

The permeation rate order in amine-PIM-1 (H_2 > CO_2 > He > O_2 > CH_4 > N_2) is different than PIM-1 and other reported modified PIMs, where CO_2 is usually the most permeable gas [5–8,13]. This is mainly due to the increased size-selectivity of the polymer, in combination with slower CO_2 diffusion [11]. There is a clear trend of decreasing permeability as a function of the conversion, and as for the conversion itself, also the permeability shows scattering in the absolute values. Since the permeability measurement of multiple specimens of the same sample is typically reproducible within a few percent [43], the observed scatter must be ascribed to the sample characteristics and is likely due to small differences in their history, which may result in variations in the free volume, traces of residual solvent, absorbed humidity, factors that strongly affect the transport properties. Indeed, the scatter significantly decreases after the methanol treatment of the membranes, which is used to reset the sample history [37].

The amine modification improves the permselectivity for the H_2/CO_2 and H_2/N_2 gas pairs, witnessing a stronger size sieving behaviour of the polymer (Fig. 7a,b and Table 2). Contrary to the original scope to improve selectivity by increasing the affinity for CO_2, higher conversion leads to a remarkable decrease in the CO_2/N_2 and CO_2/CH_4 permselectivities (Fig. 7c,d and Table 2). This indicates that the increased size-selectivity has a stronger effect on the overall transport parameters than the increased sorption selectivity for CO_2 (Fig. 4). This is confirmed by the very strong decrease of CO_2 diffusion (SI Fig. 7a) and, for instance, by the very large increase in H_2/CO_2 diffusion selectivity (SI Fig. 8a) as a function of the conversion.

Upon aging, the CO_2 permeability of AM_93b decreases by only 12%

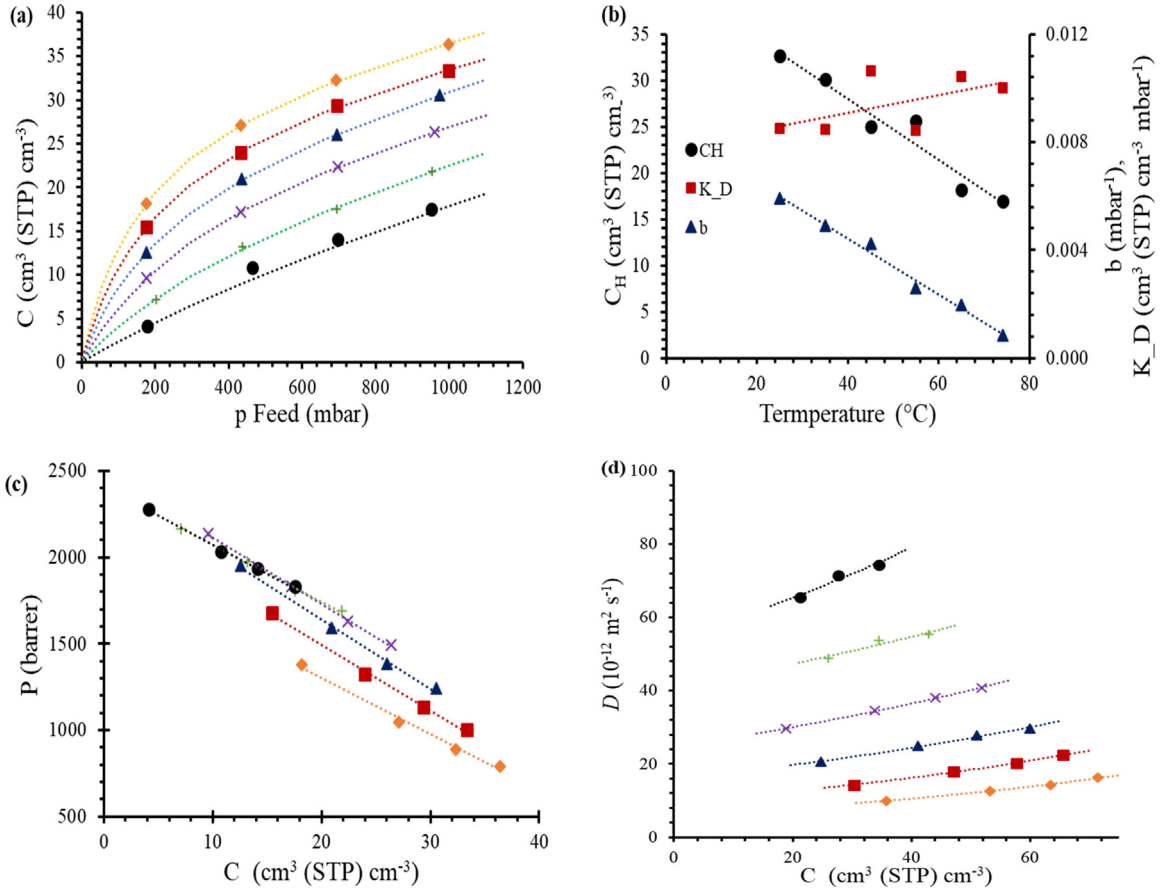

Fig. 9. (a) Sorption isotherms, (b) temperature dependence of the dual mode sorption parameters (Eq. (11)), (c) concentration dependence of the permeability and (d) concentration dependence of the diffusion coefficient as determined by the pressure-increase method for CO_2 in membrane AM_93a. (◆) 25, (■) 35, (▲) 45, (×) 55, (+) 65, and (•) 75 °C.

in the first 42 days from the MeOH treatment (data not shown in the table). This is about four times lower than the reduction of the CO_2 permeability in PIM-1 membrane after only 27 days of aging after a similar ethanol treatment [44]. This means that amine-PIM-1 is much more stable over time than the parent polymer, probably as a result of its lower free volume and inter- and intramolecular hydrogen bonding.

3.3.3. *Influence of temperature and pressure on the gas transport*

The distinct dual mode sorption behaviour and the high affinity of amine-PIM-1 is specific for CO_2, especially at low pressure. Gas permeation measurements at pressures between 0.1 and 1 bar in the time lag instrument, show a strong pressure dependence of the permeability of CO_2, whereas the permeability of other gases is virtually constant (SI Fig. 9). The strong affinity of the membrane for CO_2 leads to a drastic increase of the solubility coefficient with decreasing pressure.

Gas permeation of membrane AM_93a was monitored at various temperatures between 15 °C and 75 °C, where the sample is chemically stable according to TGA analysis (SI Fig. 10). A slight weight loss observed in TGA below 100 °C can be ascribed to desorption of gases and humidity from the sample after it has been exposed to the atmosphere, while degradation starts only above 350 °C, against 450 °C for PIM-1. In the absence of thermal transitions, the diffusivity coefficients usually increase with temperature [45] and the solubility decreases, while the permeability depends on the relative contribution of both effects. These trends are indeed observed for all gases (Fig. 8a,c,e). An anomaly is the lower diffusion coefficient for CO_2 than for N_2, which persists over the entire temperature range, and the unusually strong increase in CO_2 permeability as a function of temperature, resulting in a nearly constant CO_2/CH_4 selectivity. The anomaly originates from the very high affinity of CO_2 for the polymer matrix, as hypothesized previously [11], affecting negatively the diffusion coefficient. However, the effect of temperature on the diffusion coefficient is normal and the diffusivity selectivity for the CO_2/CH_4 gas pair decreases with increasing temperature, whereas there is a remarkable increase in the CO_2/CH_4 solubility selectivity. For comparison, the O_2/N_2 permselectivity and diffusivity selectivity decrease, whereas the solubility selectivity is constant with temperature. The origin of this phenomenon is that the CO_2 affinity of the polymer is so high that most of the Langmuir sites are already saturated at relatively low pressures. Therefore, the temperature increase does not lead to the expected strong decrease in CO_2 solubility, and the solubility of the other gases decreases more than that of CO_2. This is very interesting in view of potential application of these membranes in industrial separations, where a temperature increase usually leads to a deterioration of the performance.

Activation energies for permeation and diffusion and the heat of sorption are given in SI Table 3. The activation energy for diffusion of all six gases is higher in amine-PIM-1 than in PIM-1 [45]. This is consistent with the observed shrinkage upon conversion into the amine, and the higher density of the latter, indicating a lower free volume in the membrane.

SI Figure 12 shows permeability, diffusion and solubility coefficients of CO_2 in amine-PIM-1 (AM_93a) as functions of temperature (from 25° to 75°C) and at different pressures (from 0.2 to 1 bar). The permeability coefficient for CO_2 increases with increasing temperature at all pressures, which is a general trend where diffusion dominates. Moreover, permeability coefficient decreases with an increased pressure at all temperatures due to the dual mode sorption behaviour [45]. The diffusion coefficient increases in an Arrhenius-like fashion, with an

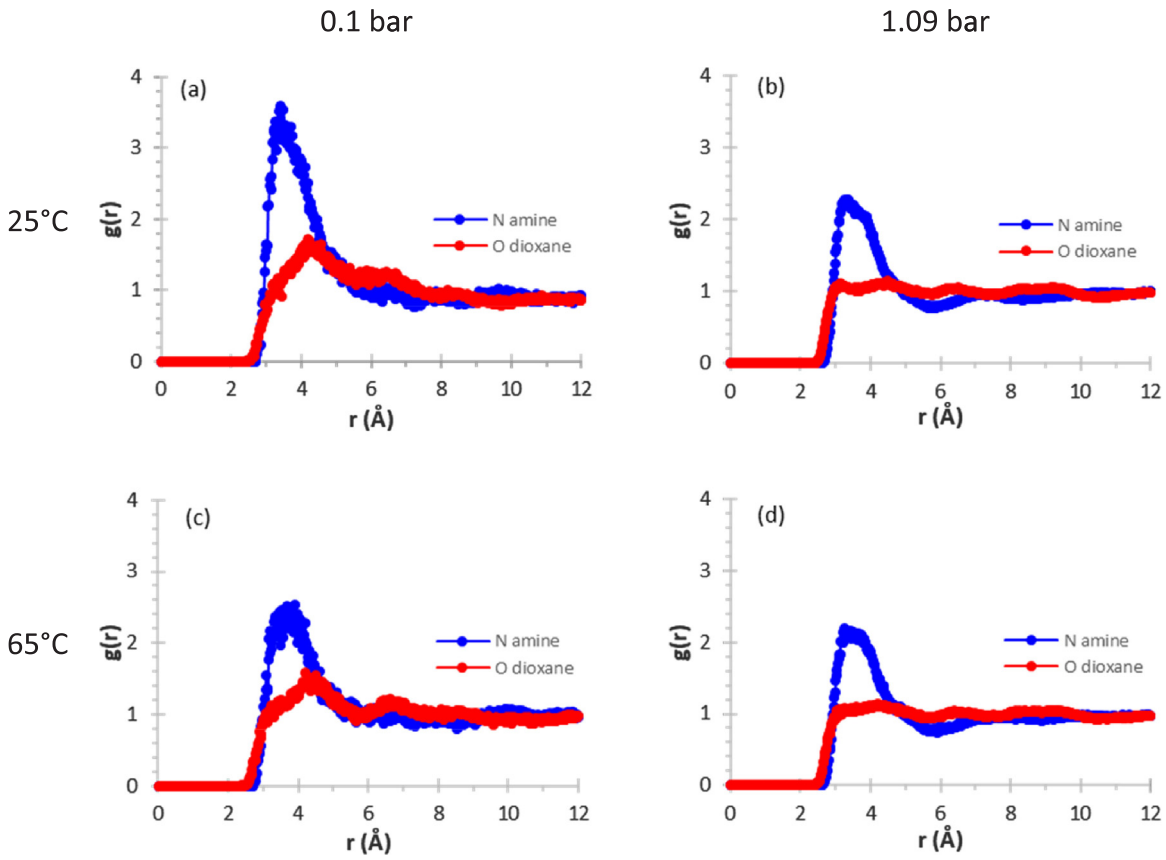

Fig. 10. Radial Distribution Function of CO_2 molecules from the amine or dioxane groups in amine-PIM-1 at: (a) 0.1 bar and 25 °C; (b) 1.09 bar and 25 °C; (c) 0.1 bar and 65 °C; (d) 1.09 bar and 65 °C.

exponential increase as a function of temperature, while the solubility decreases. For qualitative comparison with the gravimetric sorption experiments, the solubility data were expressed in terms of the dual mode sorption model (Eq. (10)), where the gas concentration in the membranes was determined from the indirectly calculated solubility by:

$$C = S \times p \tag{11}$$

The resulting sorption isotherms of CO_2 at the different temperatures (Fig. 9a) show a significant decrease in the dual mode behaviour and a decrease in the initial slope with increasing temperature. For other polymers such a transition from dual mode behaviour to Henry behaviour is common for much broader pressure ranges, when approaching the glass transition temperature [46]. In this case, it is already evident at much lower pressures and far below the glass transition temperature due to the very high affinity of amine-PIM-1 for CO_2 in the ultramicroporosity region. Qualitatively, the effect of temperature is reflected in a decreasing Langmuir site sorption capacity and lower gas-polymer affinity (Fig. 9b) with increasing temperature. The plots of the diffusion and permeation coefficients as a function of the gas concentration in the membrane clearly show that both parameters are strongly concentration dependent (Fig. 9c,d). Therefore, the concentration independency of P and D assumed in the derivation of the time-lag procedure is strictly not correct for polymers with such strong dual mode behaviour, and the data should be used only for qualitative comparison. More rigorous studies would require numerical methods for calculation of the concentration profile across the membrane and the concentration-dependent transport parameters.

3.4. Molecular modelling

3.4.1. Molecular dynamics simulations

The radial distribution function, *g(r)*, related to specific interactions between the CO_2 molecules and the amine-N and dioxane-O functional groups of the membrane, calculated from molecular dynamics runs, support the experimental observations of the very high CO_2 solubility at low pressure (Fig. 10). The curve of *g(r)* indicates the local probability density of finding type B atoms at a distance r from type A atoms, averaged over the equilibrium density [47], and is defined by the equation:

$$g(r) = \frac{n_B/4\pi r^2 dr}{N_B/V} \tag{12}$$

where N_B is the total number of type B atoms, V is the total volume, n_B is the number of type B atoms lying at a distance r from atom A, considering a shell of thickness dr.

In all cases, there is a strong peak at about 3 Å from the amino groups, witnessing the interaction between the amine-groups and the polarized C=O bonds of the CO_2 molecules. On the other hand, the much smoother curve for the dioxane/CO_2 radial distribution indicates a weaker interaction. This amine/CO_2 interaction decreases both with increasing pressure and with increasing temperature. At higher temperature, the interaction between the amine groups and CO_2 decreases due to the intensification of the vibrational modes, whereas at higher pressure the interaction decreases by the formation of multi- shells due to the large number of molecules of CO_2 in the polymeric model at 1 bar as observed from experimental sorption.

CO_2 molecules are distributed through the polymeric matrix occupying the Langmuir sites and forming multi-shells. The Langmuir sorption sites have strong affinity whilst the CO_2 molecules of the multi-shell move more freely. Quantum Mechanics confirm the selective interaction between the amine functional group and CO_2. The CO_2/amine-PIM-1 noncovalent interaction has an energy of about − 2 kcal/mol, falling in the range of weak hydrogen bonding, while N_2 and CH_4 do not interact significantly with the monomer.

4. Conclusions

Borane dimethyl sulphide complexes can be used to reduce the nitrile groups in PIM-1 to primary amines, yielding amine-PIM-1. The degree of conversion can be controlled by the reaction temperature and the reaction time on both PIM-1 powder and PIM-1 membranes, as characterized by ATR-IR, solid state ^{13}C-NMR, Raman spectroscopy, elemental analysis and TGA.

The PIM-1 permeability progressively decreases with increasing conversion to the amine. Time-lag and sorption kinetics measurements evidence that this decrease is mainly diffusivity controlled. This behaviour is stronger for gases with larger molecular dimensions and is exceptionally strong for carbon dioxide. The presence of the amine functional groups leads to a decrease in the available free volume and also induces noncovalent interactions with carbon dioxide. The strong interaction with CO_2, confirmed by molecular modelling, leads to the nearly complete saturation of the Langmuir sorption sites at relatively low CO_2 pressures. Comprehensive analysis of the effect of temperature and pressure reveals the origin of the anomalous behaviour of CO_2 and further indicates the limits of the time lag measurements for the determination of the transport properties of polymers with strong dual mode sorption behaviour. This work confirms the introduction of amine groups into PIMs as a powerful tool to tailor their transport properties.

Acknowledgements

The work leading to these results has received funding from the European Union's Seventh Framework Program (FP7/2007–2013) under grant agreements n° 608490, project M^{4}CO$_2$ and n° 228631, project DoubleNanoMem. Financial support was also received from the Czech specific university research (MŠMT No. 20-SVV/2017). The University of Manchester is grateful to the Micromeritics grant program for provision of an ASAP 2050 surface area and porosity analyser.

Appendix A. Supplementary material

Supplementary data associated with this article can be found in the online version at http://dx.doi.org/10.1016/j.memsci.2018.03.039.

References

[1] B. Ghalei, K. Sakurai, Y. Kinoshita, K. Wakimoto, A.P. Isfahani, Q. Song, K. Doitomi, S. Furukawa, H. Hirao, H. Kusuda, S. Kitagawa, E. Sivaniah, Enhanced selectivity in mixed matrix membranes for CO_2 capture through efficient dispersion of amine-functionalized MOF nanoparticles, Nat. Energy 2 (2017) 17086, http://dx.doi.org/10.1038/nenergy.2017.86.

[2] H.A. Patel, J. Byun, C.T. Yavuz, Carbon dioxide capture adsorbents: chemistry and methods, ChemSusChem 10 (2017) 1303–1317, http://dx.doi.org/10.1002/cssc.201601545.

[3] P.M. Budd, E.S. Elabas, B.S. Ghanem, S. Makhseed, N.B. McKeown, K.J. Msayib, C.E. Tattershall, D. Wang, Solution-processed, organophilic membrane derived from a polymer of intrinsic microporosity, Adv. Mater. 16 (2004) 456–459, http://dx.doi.org/10.1002/adma.200306053.

[4] P.M. Budd, B.S. Ghanem, S. Makhseed, N.B. McKeown, K.J. Msayib, C.E. Tattershall, Polymers of intrinsic microporosity (PIMs): robust, solution-processable, organic nanoporous materials, Chem. Commun. (Camb.). 10 (2004) 230–231, http://dx.doi.org/10.1039/b311764b.

[5] N. Du, H.B. Park, G.P. Robertson, M.M. Dal-Cin, T. Visser, L. Scoles, M.D. Guiver, Polymer nanosieve membranes for CO_2-capture applications, Nat. Mater. 10 (2011) 372–375, http://dx.doi.org/10.1038/nmat2989.

[6] N. Du, G.P. Robertson, M.M. Dal-Cin, L. Scoles, M.D. Guiver, Polymers of intrinsic microporosity (PIMs) substituted with methyl tetrazole, Polymer (U. Kingd.). 53 (2012) 4367–4372, http://dx.doi.org/10.1016/j.polymer.2012.07.055.

[7] N. Du, G.P. Robertson, I. Pinnau, M.D. Guiver, Polymers of intrinsic microporosity derived from novel disulfone-based monomers, Macromolecules 42 (2009) 6023–6030, http://dx.doi.org/10.1021/ma900898m.

[8] C.R. Mason, L. Maynard-Atem, N.M. Al-Harbi, P.M. Budd, P. Bernardo, F. Bazzarelli, G. Clarizia, J.C. Jansen, Polymer of intrinsic microporosity incorporating thioamide functionality: preparation and gas transport properties, Macromolecules 44 (2011) 6471–6479, http://dx.doi.org/10.1021/ma200918h.

[9] P. Yanaranop, B. Santoso, R. Etzion, J. Jin, Facile conversion of nitrile to amide on polymers of intrinsic microporosity (PIM-1), Polym. (Guildf.). 98 (2016) 244–251, http://dx.doi.org/10.1016/j.polymer.2016.06.041.

[10] H.A. Patel, C.T. Yavuz, Noninvasive functionalization of polymers of intrinsic microporosity for enhanced CO_2 capture, Chem. Commun. 48 (2012) 9989–9991, http://dx.doi.org/10.1039/C2CC35392J.

[11] C.R. Mason, L. Maynard-Atem, K.W.J. Heard, B. Satilmis, P.M. Budd, K. Friess, M. Lanc, P. Bernardo, G. Clarizia, J.C. Jansen, Enhancement of CO_2 Affinity in a Polymer of Intrinsic Microporosity by Amine Modification, Macromolecules 47 (2014), pp. 1021–1029, http://dx.doi.org/10.1021/ma401869p.

[12] B. Satilmis, P.M. Budd, Base-catalysed hydrolysis of PIM-1: amide versus carboxylate formation, RSC Adv. 4 (2014) 52189–52198, http://dx.doi.org/10.1039/C4RA09907A.

[13] R. Swaidan, B.S. Ghanem, E. Litwiller, I. Pinnau, Pure- and mixed-gas CO_2/CH_4 separation properties of PIM-1 and an amidoxime-functionalized PIM-1, J. Memb. Sci. 457 (2014) 95–102, http://dx.doi.org/10.1016/j.memsci.2014.01.055.

[14] B. Satilmis, M.N. Alnajrani, P.M. Budd, Hydroxyalkylaminoalkylamide PIMs: selective Adsorption by Ethanolamine- and Diethanolamine-Modified PIM-1, Macromolecules 48 (2015) 5663–5669, http://dx.doi.org/10.1021/acs.macromol.5b01196.

[15] B. Santoso, P. Yanaranop, H. Kang, I.K.H. Leung, J. Jin, A critical update on the synthesis of carboxylated polymers of intrinsic microporosity (C-PIMs), Macromolecules 50 (2017) 3043–3050, http://dx.doi.org/10.1021/acs.macromol.7b00344.

[16] K. Friess, V. Hynek, M. Šípek, W.M. Kujawski, O. Vopička, M. Zgažar, M.W. Kujawski, Permeation and sorption properties of poly(ether-block-amide) membranes filled by two types of zeolites, Sep. Purif. Technol. 80 (2011) 418–427, http://dx.doi.org/10.1016/j.seppur.2011.04.012.

[17] O. Vopička, K. Friess, V. Hynek, P. Sysel, M. Zgažar, M. Šípek, K. Pilnáček, M. Lanč, J.C. Jansen, C.R. Mason, P.M. Budd, Equilibrium and transient sorption of vapours and gases in the polymer of intrinsic microporosity PIM-1, J. Memb. Sci. 434 (2013) 148–160, http://dx.doi.org/10.1016/j.memsci.2013.01.040.

[18] J. Crank, The mathematics of diffusion, 2nd ed, Clarendon Press, Oxford, 1975.

[19] J.C. Jansen, K. Friess, E. Drioli, Organic vapour transport in glassy perfluoropolymer membranes: a simple semi-quantitative approach to analyze clustering phenomena by time lag measurements, J. Memb. Sci. 367 (2011) 141–151, http://dx.doi.org/10.1016/j.memsci.2010.10.063.

[20] M.R. Khdhayyer, E. Esposito, A. Fuoco, M. Monteleone, L. Giorno, J.C. Jansen, M.P. Attfield, P.M. Budd, Mixed matrix membranes based on UiO-66 MOFs in the polymer of intrinsic microporosity PIM-1, Sep. Purif. Technol. 173 (2017) 304–313, http://dx.doi.org/10.1016/j.seppur.2016.09.036.

[21] Accelrys Software Inc., P. U. G. P. s. BIOVIA (ex Material Studio 7. 0) package. Classical simulation theory section. Sorption User Guide, 2013.

[22] H. Sun, COMPASS: an ab initio force-field optimized for condensed-phase ApplicationssOverview with details on alkane and benzene compounds, J. Phys. Chem. B. 102 (1998) 7338–7364.

[23] L. Zhang, W. Fang, J. Jiang, Effects of residual solvent on membrane structure and gas permeation in a polymer of intrinsic microporosity: insight from atomistic simulation, J. Phys. Chem. C. 115 (2011) 11233–11239, http://dx.doi.org/10.1021/jp2029888.

[24] L. Zhao, D. Zhai, B. Liu, Z. Liu, C. Xu, W. Wei, Y. Chen, J. Gao, Grand canonical Monte Carlo simulations for energy gases on PIM-1 polymer and silicalite-1, Chem. Eng. Sci. 68 (2012) 101–107, http://dx.doi.org/10.1016/j.ces.2011.09.017.

[25] K.-S. Chang, K.-L. Tung, Y.-F. Lin, H.-Y. Lin, Molecular modelling of polyimides with intrinsic microporosity: from structural characteristics to transport behaviour, RSC Adv. 3 (2013) 10403–10413, http://dx.doi.org/10.1039/C3RA40196K.

[26] O. Hölck, M. Böhning, M. Heuchel, M.R. Siegert, D. Hofmann, Gas sorption isotherms in swelling glassy polymers—Detailed atomistic simulations, J. Memb. Sci. 428 (2013) 523–532, http://dx.doi.org/10.1016/j.memsci.2012.10.023.

[27] M. Heuchel, D. Fritsch, P.M. Budd, N.B. McKeown, D. Hofmann, Atomistic packing model and free volume distribution of a polymer with intrinsic microporosity (PIM-1), J. Memb. Sci. 318 (2008) 84–99, http://dx.doi.org/10.1016/J.MEMSCI.2008.02.038.

[28] D.N. Theodorou, U.W. Suter, Detailed molecular structure of a vinyl polymer glass, Macromolecules 18 (1985) 1467–1478, http://dx.doi.org/10.1021/ma00149a018.

[29] D.N. Theodorou, U.W. Suter, Atomistic modeling of mechanical properties of polymeric glasses, Macromolecules 19 (1) (1986) 139–154.

[30] H.J.C. Berendsen, J.P.M. Postma, W.F. van Gunsteren, A. DiNola, J.R. Haak, Molecular dynamics with coupling to an external bath, J. Chem. Phys. 81 (1984) 3684–3690, http://dx.doi.org/10.1063/1.448118.

[31] M. Valiev, E.J. Bylaska, N. Govind, K. Kowalski, T.P. Straatsma, H.J.J. Van Dam, D. Wang, J. Nieplocha, E. Apra, T.L. Windus, W.A. De Jong, NWChem: a comprehensive and scalable open-source solution for large scale molecular simulations, Comput. Phys. Commun. 181 (2010) 1477–1489, http://dx.doi.org/10.1016/j.cpc.2010.04.018.

[32] A.D. Becke, Density-functional thermochemistry. III. The role of exact exchange, J. Chem. Phys. 98 (1993) 5648–5652, http://dx.doi.org/10.1063/1.464913.

[33] C. Lee, W. Yang, R.G. Parr, Development of the Colle-Salvetti correlation-energy formula into a functional of the electron density (https://link.aps.org/doi/), Phys. Rev. B. 37 (1988) 785–789, http://dx.doi.org/10.1103/PhysRevB.37.785.

[34] A. Fuoco, S. Galier, H. Roux-deBalmann, G. De Luca, Correlation between macroscopic sugar transfer and nanoscale interactions in cation exchange membranes, J. Memb. Sci. 493 (2015) 311–320, http://dx.doi.org/10.1016/j.memsci.2015.06.028.

[35] S. Simon, M. Duran, J.J. Dannenberg, How does basis set superposition error change the potential surfaces for hydrogen-bonded dimers? J. Chem. Phys. 105 (1996) 11024–11031, http://dx.doi.org/10.1063/1.472902.

[36] H.C. Brown, Y.M. Choi, S. Narasimhan, Selective reductions. 29. A simple technique to achieve an enhanced rate of reduction of representative organic compounds by

borane-dimethyl sulfide, J. Org. Chem. 47 (1982) 3153–3163, http://dx.doi.org/10.1021/jo00137a025.
[37] P.M. Budd, N.B. McKeown, B.S. Ghanem, K.J. Msayib, D. Fritsch, L. Starannikova, N. Belov, O. Sanfirova, Y. Yampolskii, V. Shantarovich, Gas permeation parameters and other physicochemical properties of a polymer of intrinsic microporosity: polybenzodioxane PIM-1, J. Memb. Sci. 325 (2008) 851–860, http://dx.doi.org/10.1016/j.memsci.2008.09.010.
[38] P. Bernardo, F. Bazzarelli, F. Tasselli, G. Clarizia, C.R. Mason, L. Maynard-Atem, P.M. Budd, M. Lanč, K. Pilnáček, O. Vopička, K. Friess, D. Fritsch, Yu.P. Yampolskii, V. Shantarovich, J.C. Jansen, Effect of physical aging on the gas transport and sorption in PIM-1 membranes, Polym. (Guildf.). 113 (2017) 283–294, http://dx.doi.org/10.1016/j.polymer.2016.10.040.
[39] E. Tocci, L. De Lorenzo, P. Bernardo, G. Clarizia, F. Bazzarelli, N.B. Mckeown, M. Carta, R. Malpass-Evans, K. Friess, K. Pilnáček, M. Lanč, Y.P. Yampolskii, L. Strarannikova, V. Shantarovich, M. Mauri, J.C. Jansen, Molecular modeling and gas permeation properties of a polymer of intrinsic microporosity composed of ethanoanthracene and Tröger's base units, Macromolecules 47 (2014) 7900–7916, http://dx.doi.org/10.1021/ma501469m.
[40] A.J. Hill, S.J. Pas, T.J. Bastow, M.I. Burgar, K. Nagai, L.G. Toy, B.D. Freeman, Influence of methanol conditioning and physical aging on carbon spin-lattice relaxation times of poly(1-trimethylsilyl-1-propyne), J. Memb. Sci. 243 (2004) 37–44, http://dx.doi.org/10.1016/j.memsci.2004.06.007.
[41] K. Nagai, T. Masuda, T. Nakagawa, B.D. Freeman, I. Pinnau, Poly[1-(trimethylsilyl)−1-propyne] and related polymers: synthesis, properties and functions, Prog. Polym. Sci. 26 (2001) 721–798, http://dx.doi.org/10.1016/S0079-6700(01)00008-9.
[42] M. Carta, P. Bernardo, G. Clarizia, J.C. Jansen, N.B. McKeown, Gas permeability of hexaphenylbenzene based polymers of intrinsic microporosity, Macromolecules 47 (2014) 8320–8327, http://dx.doi.org/10.1021/ma501925j.
[43] I. Rose, C.G. Bezzu, M. Carta, B. Comesaña-Gándara, E. Lasseuguette, M.C.C. Ferrari, P. Bernardo, G. Clarizia, A. Fuoco, J.C. Jansen, K.E.E. Hart, T.P. Liyana-Arachchi, C.M. Colina, N.B. McKeown, Polymer ultrapermeability from the inefficient packing of 2D chains, Nat. Mater. 16 (2017) 932–937, http://dx.doi.org/10.1038/nmat4939.
[44] P. Bernardo, F. Bazzarelli, F. Tasselli, G. Clarizia, C.R. Mason, L. Maynard-Atem, P.M. Budd, M. Lanč, K. Pilnáček, O. Vopička, K. Friess, D. Fritsch, Y.P. Yampolskii, V. Shantarovich, J.C. Jansen, Effect of physical aging on the gas transport and sorption in PIM-1 membranes, Polym. (Guildf.). 113 (2017) 283–294, http://dx.doi.org/10.1016/J.POLYMER.2016.10.040.
[45] P. Li, T.S. Chung, D.R. Paul, Temperature dependence of gas sorption and permeation in PIM-1, J. Memb. Sci. 450 (2014) 380–388, http://dx.doi.org/10.1016/J.MEMSCI.2013.09.030.
[46] W.J. Koros, D.R. Paul, CO_2 sorption in poly(ethylene terephthalate) above and below the glass transition, J. Polym. Sci. Polym. Phys. Ed. 16 (1978) 1947–1963, http://dx.doi.org/10.1002/pol.1978.180161105.
[47] J.M. Haile, Molecular Dynamics Simulation: elementary Methods, Wiley, New York, 1997.